Aspheric optical surface profiling based on laser scanning and auto-collimation[a)]

Hongbo Xie,[1] Min Jiang,[1] Yao Wang,[1] Xiaotian Pang,[1] Chao Wang,[2] Yongpeng Su,[1] and Lei Yang[1, b)]

[1)] *College of Precision Instrument and Opto-electronics Engineering, Tianjin University*
Key Laboratory of Optoelectronics Information Technology, Ministry of Education, Tianjin, 300072, China.
[2)] *School of Engineering and Digital Arts, University of Kent, Canterbury CT2 7NT, UK*

(Dated: 19 October 2017)

Nowadays the utilization of aspheric lenses has become more and more popular, enabling highly increased degree of freedom for optical design and simultaneously improving the performance of optical systems. Fast and accurate surface profiling of these aspheric components is a real demand in characterization and optimization of the optical systems. In this paper, a novel and simple surface profiler instrument is designed and developed to fulfill the ever increasing need of testing axially symmetric aspheric surface. The proposed instrument is implemented based on a unique mapping between the position and rotation angle of reflective mirror in optical path and the coordinate of reflection point on the surface during rapid laser beam scanning. High accuracy of the proposed surface profiling method is ensured by high-resolution grating guide rail, indexing plate and position sensitive detector based on laser auto-collimation and beam center-fitting. Testing the meridian line of both a convex and a concave surfaces has been experimentally demonstrated using the developed instrument. In comparison to tested results from conventional image measuring instrument and coordinate measuring machine, coefficient of determination better than 0.99999 and RMS less than 1.5 μm have been achieved, which validates the feasibility of this method. Analysis on the systematic error is beneficial to further improve its measurement accuracy. The presented instrument—essentially builds on the geometrical optics technique—provides a powerful tool to measure the aspheric surfaces quickly and accurately with stable structure and simple algorithm.

PACS numbers: 07.60.-j, 42.15.-i, 42.15.Eq, 42.79.Bh
Keywords: Aspheric surface; Axially symmetric; Meridian line; Laser scanning and auto-collimation; Beam center-fitting

I. INTRODUCTION

Aspheric lenses have been widely used for decades owing to its unique capability to eliminate optical aberrations inherent to spherical lens systems and also reduce other optical aberrations such as astigmatism[1]. Compared to classical spherical optical design, an aspheric lens makes it possible to significantly reduce the number of elements, and therefore size and weight of an optical system[2–4]. Characterizing the desired shape of individual aspheric mirrors or lenses is crucially important in optical design, processing and application[5]. In particular, quality control in fabrication process, makes 3D optical surface profiling of aspheric lenses a real demand.[6].

[a)] Supported by the Seed Foundation of Tianjin University (No. 2017XZS-0026)
[b)] Electronic mail: yanglei@tju.edu.cn

As a typical testing method for aspheric surfaces, a stylus profilometer can be used for the rough surface and smooth surface[7]. However, it always takes much time while tracing the surface and limited by the dimension. Another favorable testing category is based on interferometry which can measure the surfaces with very high accuracy[8]. Among them, null testing methods, such as computer generated hologram (CGH), have been successfully applied to measurement of difficult surfaces[9,10]. The drawback of such metrology method is that a matching null optics has to be fabricated for every design elements, which is highly time and cost consuming[10]. An alternative way is non-null testing, such as sub-aperture stitching[11], which offers flexible measurement results with acceptable accuracy and allow general test of aspheric lenses in some sense[12,13]. Nevertheless, interferometry based solutions are usually composed of complex and expensive optical structures and always require sophisticated algorithm to recover the whole profiles[14]. Consequently, other measuring technologies, based on geometric ray-testing, with its unique ability of simple, convenient and low-cost are still extremely attractive for fabrication and production of high-quality aspheric lenses[15].

Most recently, aiming at profile measurement of optical surfaces, scanning deflectometric systems have been well developed in terms of the geometric relationship between scanning rays[15–17]. K. Ishikawa et al. reported a scanning deflectometry using a rotating commercial autocollimator with complementary metal-oxide semiconductor (CMOS) as a light-receiving element, which successfully measured aspheric lenses with extremely high-accuracy[16]. However, rotating entire autocollimator limits the measurement range of deflectometry, especially for the optical surfaces with large slope changes. Therefore, an alternative approach to enlarge the rotating angle and improve the translational and rotational speed of autocollimator is still highly essential to the developed deflectometric tester.

In this work, we proposed and demonstrated a laser scanning and auto-collimation tester (LSACT) and its light recognizing and locating is accomplished by home-made autocollimator, being composed of a reflective mirror (RM) and a position sensitive detector (PSD). Compared to operating the whole autocollimator, rotating a reflective mirror provides faster scanning and larger rotatory angle. Instead of using CMOS detector, PSD with higher resolution is employed to capture the position of scanning light.

As a feasible measurement technique for characterizing aspheric optical surfaces with axially symmetric structure, LSACT was developed by means of geometrical relationships between scanning beams and meridian line of the surface under test. In LSACT, collimated laser beam illuminates one point on the surface under test. The spatial coordinate of the point can be uniquely determined from the position and rotation angle (can be defined as pose) of a RM that guarantees perfect normal incidence to the optical surface. The entire meridian line of the surface can be reconstructed through laser beam scanning. Accurately measuring the rotation angle of the reflection mirror during each scanning step is crucial to achieve high-accuracy surface profiling. This is ensured by using a high-resolution PSD which can precisely judge the angle of reflected scanning beam.

In view of the auto-collimation and beam center-fitting principle, when the reflected scanning beam exactly locates at the center of PSD, totally coinciding of incident and reflected beam definitely determines the relationship between position of scanned point on the surface and the RM. To measure the shape of surface, a close form calculation model has been developed utilizing the movement coordinate and rotary angle of the RM. Therefore, our method completely eliminates the need for calibration plates or reference surfaces, and features compact structure and simple algorithm. Furthermore, the presented approach provides a versatile solution for various aspheric surfaces (concave or convex) with different sizes.

The remainder of this article is structured as follows. In Section II, we first describe the operation principle of the proposed LSACT system. We apply it in Sec. III to study on the algorithm of performing the profile using experimental parameters. More experimental details are given in Sec. IV, where results of measuring two different aspheric components are reported. Finally, we summarize our findings and discuss implications and future directions for this work.

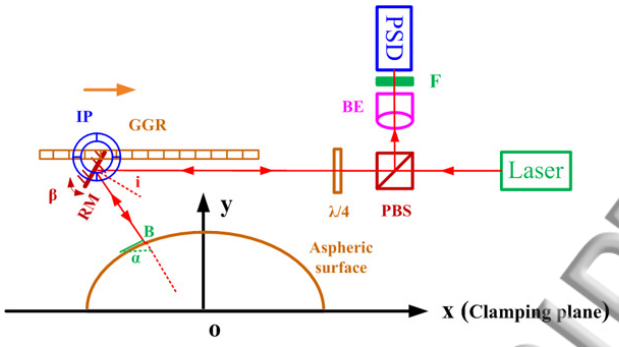

FIG. 1. Schematic diagram of the laser scanning and auto-collimation tester for aspheric surface. RM, reflective mirror; GGR, grating guide rail; IP, indexing plate; BE, beam expander; PSD, position sensitive detector; F, filter; PBS, polarization beam splitter; $\lambda/4$, quarter-wave plate. The principle we should follow is recording the rotation angle of RM when guaranteeing the scanning beam vertically incidents on the surface and comes back along the original optical path.

II. PRINCIPLE AND METHOD

Fig.1 illustrates diagrammatically the key principle on which the tester is based. It mainly consists of a laser, PSD, RM, scanning device and the surface fixed at clamping plane. The instrument is designed basically to measure the contour profile of fixed surface utilizing the coordinate of discrete points, originated by recording the horizontal movement and rotation of the reflective mirror in the arrangement. Without loss of generality, we assume that the surface is axially symmetric. Measuring the aspheric surface can be simplified by depicting the outline of meridian plane and then symmetrically rotating it.

In practice, the p-polarized 532 nm light beam emitted from the laser (Model: MGL-S-532-B), passing through the polarization beam splitter (PBS) and $\lambda/4$ plate, incidents on the surface by RM and comes back to RM again after reflected by the surface. Then, after properly adjusted by $\lambda/4$ plate, reflected s-polarized light passes through filter (F) and beam expander (BE), and directly hits on the PSD. On account of the auto-collimation and beam center-fitting principle, the scanning beam can return along the original path in the context of light beam being aligned with the PSD center, when the RM rotates a special angle defined as β (see Fig. 1). In order to reduce the spot size of light injecting on PSD, a BSL with 4× Kepler telescope structure, whose exit-pupil diameter is less than 9.5 mm, is introduced to the system. A photograph of the constructed LSACT in the lab is shown in Fig. 2.

Before measurement, two alignment procedure, assuring the coincidence of rotation axis for RM, IP and motor and guaranteeing the direction of GGR being parallel to the clamping plane, should be focused on. In the first procedure, three photodiodes with small active-area (First Sensor, PC5-6-TO5) are put in different locations in x-y plane and connected to oscilloscope (Tektronix TPS2014) for capturing outputting signal. When the RM is turned 10 rounds continuously, carefully adjusting the relative position of RM, IP and motor to guarantee reflected light incomes into three photodiodes in every round, which indicates the coaxial of RM, IP and motor. In the second procedure, a standard optical flat is laid on the clamping plane to replace the sample. The RM mounted on the GGR, fixed at 45^o all the time, is moved from starting to ending position. Maintaining the coincidence of incident and reflected light in the movement of RM proves the direction of GGR in parallel with the clamping plane.

Here the measurement process is presented in more detail as follows. Firstly, the electrical motor controlled by a high-precison grating guide rail (GGR) drives the RM to move with uniform steps. Then, at each point, RM mounted on the indexing plate (IP) is continuously drove by a rotary motor. When the returned scanning beam exactly hit the center position of the PSD, rotary motor is turned off and the pose of RM is simultaneously recorded by data acquisition system. Finally, after scanning all the points of tested surface, the profile

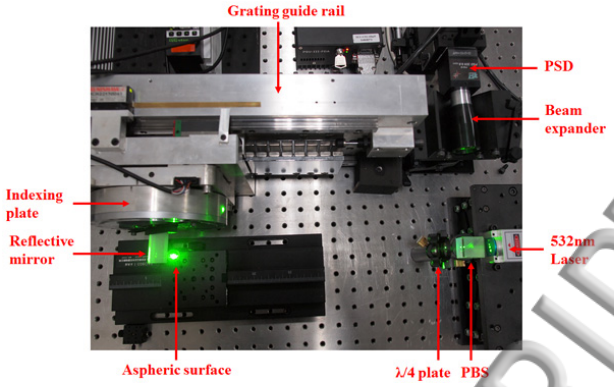

FIG. 2. A photograph of experimental setup of the LSACT in the lab.

of surface could be described by utilizing the linear displacement x and rotation angle β of RM.

For clarity, the geometrical relationship between the scanning light and RM will be analyzed. The angle of laser beam incidenting on RM, rotation angle of RM and angle of tangent line passing point B are defined as i, β and α in xoy Cartesian coordinate system, respectively, when the initial rotation angle of RM is definitely set at 45^o for each measured point. Considering the reflection law and optical features of mirror[18], the equations of $i = \frac{1}{2}(90^o - \alpha)$ and $\beta = \frac{1}{2}(90^o - 2i)$ can be obtained. Then, the relationship of essential angles in the setup is found to be

$$\alpha = 2\beta \tag{1}$$

Meanwhile, the diameter of measured aspheric lens can be deduced as

$$D = 2(L - \frac{H}{\tan(90^o - 2\beta)}) \tag{2}$$

where H is the coordinate of center of RM in y-axis and L denotes the displacement value of RM.

Accordingly, provided that the GGR selected with proper length and the rotation angle of RM exceeding 45 ^{o} are both satisfied, the commercial aspheric lens commonly ranging from 10 mm to 150 mm is within the measurement range of our LSACT. What's more, the precision of PSD, linear displacement and rotation of mirror greatly determine the measuring accuracy of surface, when the position resolution, precision of GGR and minimum step of IP are set at 1 μm, 1 μm and $0.16''$, respectively.

III. ALGORITHM

In this section, in order to find the geometrical relationship between the measured points in the surface and experimental parameters, the exact coordinates of measured point are solved under the basic assumption that aspheric contour consists of massive amount of arcs. More specifically, the arc, successively connecting to form the contour, is part of osculating circle of contour whose centre located at y-axis.

The geometrical model of LSACT under consideration is detailed depicted in Fig. 3. Starting with point A_0, RM is moved by electrical motor with Δx step once a time, which is then precisely located at special points A_n $(n = 0, 1, 2...)$. At a fixed location A_n, RM reflects the incidenting light onto the surface with point B_n and also reflect the light to detector with special rotating angle β_n. We assume O_nB_n is the extension line of A_nB_n, which intersects x-axis at M_n and y-axis at O_n, respectively. In addition, O_n is defined as the center of osculating circle, which inscribes the surface and goes through point B_n.

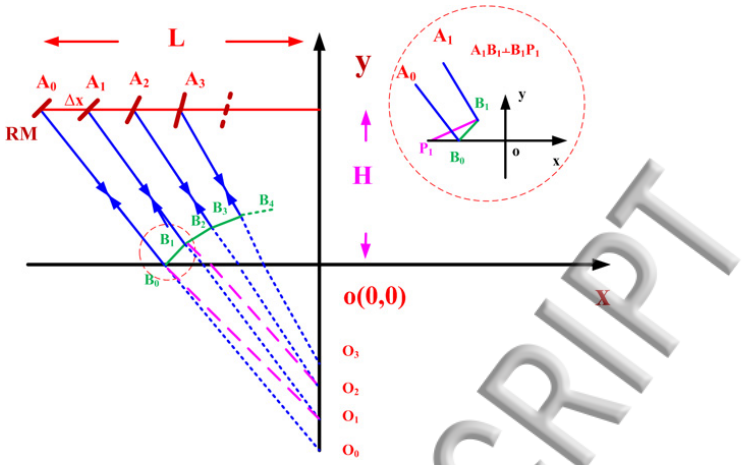

FIG. 3. Principle of measuring the optical surface of aspheric using laser scanning and auto-collimation method. A_0, A_1, A_2 ... represent the position of RM at each movement while B_0, B_1, B_2 ... stand for the measured points on the surface. The inset map is amplified detail of the part marked by red circle, in which line A_1B_1 is perpendicular to line B_1P_1.

In general, the contour line, connecting all the points B_n, accurately plots the meridional plane of measured component. Hence the purpose of following calculation is to deduce the expressive coordinate of B_n $(x_n,\ y_n)$, which is the intersection of line O_nB_n and string $B_{n-1}B_n$. Moreover, the slope of line O_nB_n is $-\cot\alpha_n$, in which α_n satisfies $\alpha_n = 2\beta_n$ (see Eq. (1)).

As an starting point, B_0 is also a critical point that is able to reflect the incidenting light into the detector at first time. Taking into consideration the slope of line O_0B_0 (O_0A_0) $(-\cot\alpha_0)$ and coordinate of $A_0(-L, H)$, the equation of O_0B_0 can be written as

$$y = -\cot\alpha_0(x + L) + H \tag{3}$$

Therefore, the coordinate of B_0 $(\frac{H}{\cot\alpha_0} - L, 0)$ is obtained.

Similarily, when we utilize the coordinate of A_1 $(H - \Delta x, L)$, the equation of line O_1B_1 can be given by

$$y = -\cot\alpha_1(x + L - \Delta x) + H \tag{4}$$

Then the corresponding coordinate of O_1 has the general form of $(0,\ H - \cot\alpha_1(L - \Delta x))$.

Hence the slope of line B_0O_1 can be represented by

$$k_1 = \frac{\cot\alpha_1(L - \Delta x) - H}{\frac{H}{\cot\alpha_0} - L} \tag{5}$$

Nextly, the focusing issue is how to find the value of $\angle B_0O_1M_1$, which is the intersection angle of line B_0O_1 and B_1O_1. Obviously,

$$\angle B_0O_1M_1 = \arctan|\frac{k_1 - k_1'}{1 + k_1k_1'}| \tag{6}$$

where $k_1' = -\cot\alpha_1$.

For clarity, the detailed geometrical relationship between line B_0B_1 and the centre of a circle O_1 is plotted in the inset of Fig. 3 (amplified structure marked by red circle). It is well known that angle of osculation is equal to half of the central angle. Therefore, angle of osculation $\angle P_1B_1B_0$ is equal to $\frac{\angle B_0O_1M_1}{2}$ and $\angle B_1B_0M_1 = \alpha_1 + \frac{\angle B_0O_1M_1}{2}$.

The equation of line B_0B_1 is given by

$$y = M_1(x + L - \frac{H}{\cot\alpha_0}) \tag{7}$$

where $M_1 = \tan\angle B_1B_0M_1$.

According to Eq. (2) and (5), the coordinate of B_1, intersection point of line B_0B_1 and O_1B_1, is transformed into

$$x_1 = \frac{H + M_1(\frac{H}{\cot\alpha_0} - L) + (\Delta x - L)\cot\alpha_1}{M_1 + \cot\alpha_1}, \tag{8a}$$

$$y_1 = \frac{HM_1 + (M_1\Delta x - \frac{M_1H}{\cot\alpha_0})\cot\alpha_1}{M_1 + \cot\alpha_1}. \tag{8b}$$

Similar to calculations above, the method is extended to arbitrary measured point, when the coordinate $(0, H - \cot\alpha_n(L - n\Delta x))$ stands for the centre of a circle O_n. The slope of line $B_{n-1}O_n$ takes the form

$$k_n = \frac{y_{n-1} - H + \cot\alpha_n(L - n\Delta x)}{x_{n-1}} \tag{9}$$

And the slope of line B_nO_n has the general form

$$k'_n = -\cot\alpha_n \tag{10}$$

On the basis of intersection angle theorem, we obtain

$$\angle B_{n-1}O_nB_n = \arctan|\frac{k_n - k'_n}{1 + k_nk'_n}| \tag{11}$$

In this case, the slope of line $B_{n-1}B_n$ is in the form

$$M_n = \tan(\alpha_n + \frac{1}{2}\arctan|\frac{\cot\alpha_n + \frac{y_{n-1}-H+\cot\alpha_n(L-n\Delta x)}{x_{n-1}}}{\frac{\cot\alpha_n(y_{n-1}-H+\cot\alpha_n(L-n\Delta x))}{x_{n-1}} - 1}|) \tag{12}$$

where $\angle B_nB_{n-1}O = \alpha_n + \frac{1}{2}\angle B_{n-1}O_nB_n$.

It is easy to show that equation of line $B_{n-1}B_n$ is given by

$$y = M_n(x - x_{n-1}) + y_{n-1} \tag{13}$$

Clearly, the equation of line B_nO_n can be written as

$$y = -\cot\alpha_n(x + L - n\Delta x) + H \tag{14}$$

After simplifying, coordinate of measured point B_n can be performed analytically and results in the following expression:

$$x_n = \frac{H - y_{n-1} + M_nx_{n-1} + (n\Delta x - L)\cot 2\beta_n}{M_n + \cot 2\beta_n}, \tag{15a}$$

$$y_n = \frac{HM_n + (y_{n-1} - M_nx_{n-1} - M_nL + M_nn\Delta x)\cot 2\beta_n}{M_n + \cot 2\beta_n}. \tag{15b}$$

Eq. (15) is a simple close-form expression that reveals functional relationship between coordinate of scanned point and fundamental coefficients of measurement in general form. As geometrical optics principle of LSACT are being recoginzed, the theory and algorithm presented here are expected to be valuable in measurement of aspheric lens that are based on the auto-collimating laser scanning.

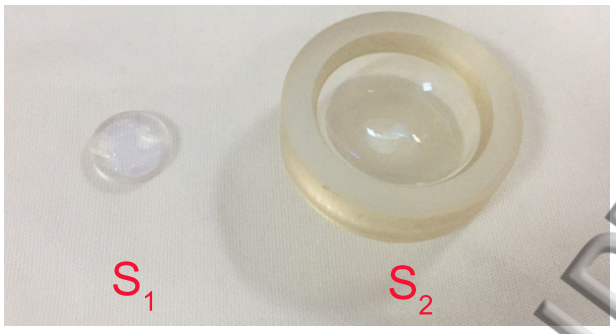

FIG. 4. Samples of a concave aspheric surface S_1 and a convex aspheric S_2. According to the datasheets supplied by manufacturer, the nominal curve was expressed as $y = \frac{x^2}{R(1+\sqrt{1-\frac{(1+k)x^2}{R^2}})} + ax^4 + bx^6 + cx^8$, where the nominal coefficients are $R = 13.0632, k = -0.572510, a = 0, b = -9.4106 \times 10^{-9}, c = 0$ for S_1 and $R = -11.148, k = -0.255925, a = 3.98141 \times 10^{-5}, b = -8.87325 \times 10^{-8}, c = 2.63198 \times 10^{-9}$ for S_2, respectively. The deviation of two samples relative to their best-fit spheres are approximately 30 μm and 70 μm, respectively.

IV. EXPERIMENT AND RESULTS

The proposed method of the LSACT was investigated experimentally when a concave and a convex aspheric lenses were characterized. The photograph and nominal data of samples are shown in Fig. 4, where the surfaces to be tested are 10.0 mm and 15.6 mm in diameter (provided by manufacturer), respectively. The significant parameter H, height of RM, in algorithm restoring the shape of surface S_1 and S_2 were set at 38.73 mm and 35.40 mm, respectively. Measuring the meridian line of sample S_1 and S_2 cost 97.2 s and 39.6 s, respectively, and the measuring speed is roughly 0.5 s per point. Final measured results and deviations between the measured data and nominal curve are shown in Fig. 5, including the restored 3D map of samples by rotating the meridian line along symmetric axis.

With the purpose of further testifying the feasibility of the presented instrument, samples of S_1 and S_2 were also measured and profiled utilizing high-precision image measuring instrument (IMI) and coordinate measuring machine (CMM), respectively. Moreover, the measuring accuracy of IMI (OGP, SmartScope ZIP 250) and CMM (Hexagon, Leitz) can achieve 1 μm and 0.5 μm, respectively. In particularly, measuring the same meridian line in different testers is ensured by starting from the marked point on the sample and accurately finding out the vertex of the aspheric lens. Comparison of measured results between LSACT and IMI, LSACT and CMM, are shown in Fig. 6 and Fig. 7, respectively, including revealing the deviation of every measured points between different methods. In addition, coefficient of determination C and root mean square (RMS) were also used to assess the proposed method.

Coefficient of determination C, describing the difference between two series of measured data, is expressed as

$$C = \frac{\sum_{i=1}^{N} PQ - \frac{\sum_{i=1}^{N} P \sum_{i=1}^{N} Q}{N}}{\sqrt{[\sum_{i=1}^{N} P^2 - \frac{(\sum_{i=1}^{N} P)^2}{N}][\sum_{i=1}^{N} Q^2 - \frac{(\sum_{i=1}^{N} Q)^2}{N}]}} \tag{16}$$

where N is the measured points. P and Q represent coordinate matrix of measured data from LSACT and other tester, respectively. The closer the coefficient C is close to 1, the more similar the two series of data are.

As a normally used indicator to depict the differences between predicted values and observed values, RMS of our measurement can be written as

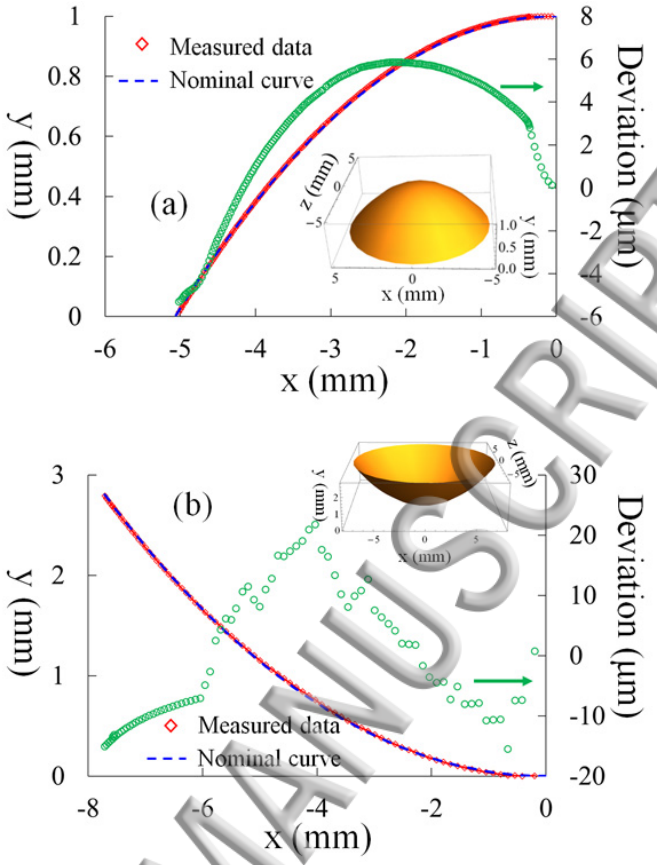

FIG. 5. Measurement results of sample S_1 and S_2 using LSACT. (a) Meridian line of sample S_1. Step of GGR $\Delta x = 0.1\ mm$, total measured points $N = 206$. (b) Meridian line of sample S_2. Step of GGR $\Delta x = 0.5\ mm$, total measured points $N = 84$. In each picture, red hollow diamond and blue dotted line, corresponding to the primary axis, represent the measured data and nominal curve, respectively. The deviation between the measured data and nominal curve is represented by green hollow circle and shown in secondary axis. The bottom right (top right) inset of (a) ((b)) is the 3D model of sample S_1 (S_2) restored by measured meridian line. According to the standard aspheric equation expressed in caption of Fig. 4, the fitting coefficients $R = 13.071511, k = -0.571931, a = 3.124813 \times 10^{-6}, b = -8.723367 \times 10^{-9}, c = 1.699320 \times 10^{-9}$ for measured meridian line of S_1 and $R = -11.173742, k = -0.265367, a = 3.951366 \times 10^{-5}, b = -7.384123 \times 10^{-8}, c = 2.591674 \times 10^{-9}$ for measured meridian line of S_2 are optimized.

$$RMS = \{\sum_{i=1}^{N} \frac{(P-Q)^2}{N}\}^{\frac{1}{2}} \tag{17}$$

The measured data of meridional line of surface S_1 and analysis of deviation for measured points are shown in Fig. 6(a) and (b), respectively. The coefficient C is as high as 0.99999 and RMS is 1.496 μm. Meanwhile, the detailed data of surface S_2 is presented in Fig. 7, where the coefficient C is 0.99999 and RMS is 1.213 μm. It is obvious that the measured data from LSACT is in agreement with the data from other methods, which indicates the accuracy of newly-designed LSACT nearly reach to the conventional surface profiler. On the other hand, the measured data from LSACT always bigger than data from CMM and IMI is an existing problem needing urgent attention.

Therefore, we analyzed the systematic error of LSACT to demonstrate the factors that cause the measured deviation and impact on the accuracy of the instrument. On account

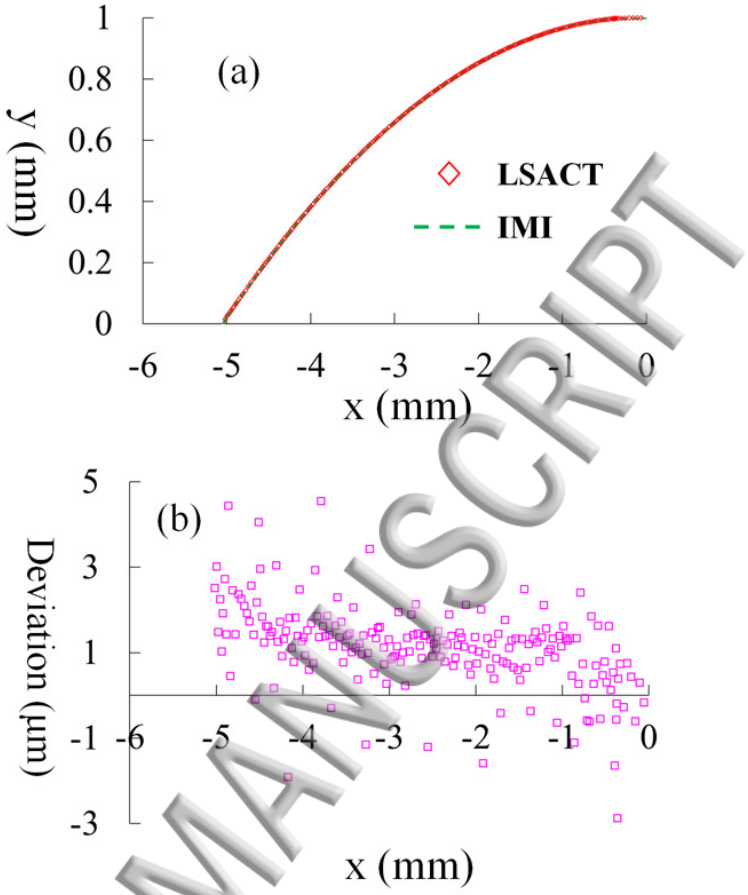

FIG. 6. Compared measured results of sample S_1 between LSACT and IMI. (a) Measured meridian line of sample S_1. The red hollow diamond represents the measured data from LSACT while the green dotted line represents the measured curve from IMI. Coefficient of determination $C = 0.99999$ and $RMS = 1.496\ \mu m$. (b) The deviation of measured data from LSACT to the IMI. Using the standard aspheric equation (shown in caption of Fig. 4), the fitting coefficients $R = 13.443191, k = -0.610865, a = 4.124813 \times 10^{-6}, b = -9.123376 \times 10^{-9}, c = 4.879131 \times 10^{-9}$ for measured meridian line in IMI are obtained.

of the principle of our instrument, rotary error of RM E_A, position error of RM E_P and measured error of H E_H are the major components of systematic error. Specifically, rotary error E_A is found to be

$$E_A = \sqrt{E_i^2 + E_c^2 + E_s^2 + (\frac{E_d}{l_t})^2} \tag{18}$$

where E_i is the error of IP ($0.16''$) while E_c is the coaxial error of RM, IP and rotary motor ($1'$). In addition, E_s represents the alignment error concerned with parallelism of GGR and clamping plane ($1'$). E_d stands for positioning error of PSD (1 μm) and l_t denotes the optical path from RM to PSD ($\sim$ 60 mm).

Meanwhile, the systematic error of surface profile can be given by[19]

$$\sigma = \sqrt{N}\sqrt{E_P^2 + (E_A H)^2 + E_H^2} \tag{19}$$

where N is the total number of measured points. E_P and E_H is 1 μm and 2 μm, respectively.

Although the position and rotary error of RM is minimized by utilizing high-performance devices and careful alignment, the large measured error of height H probably causes the

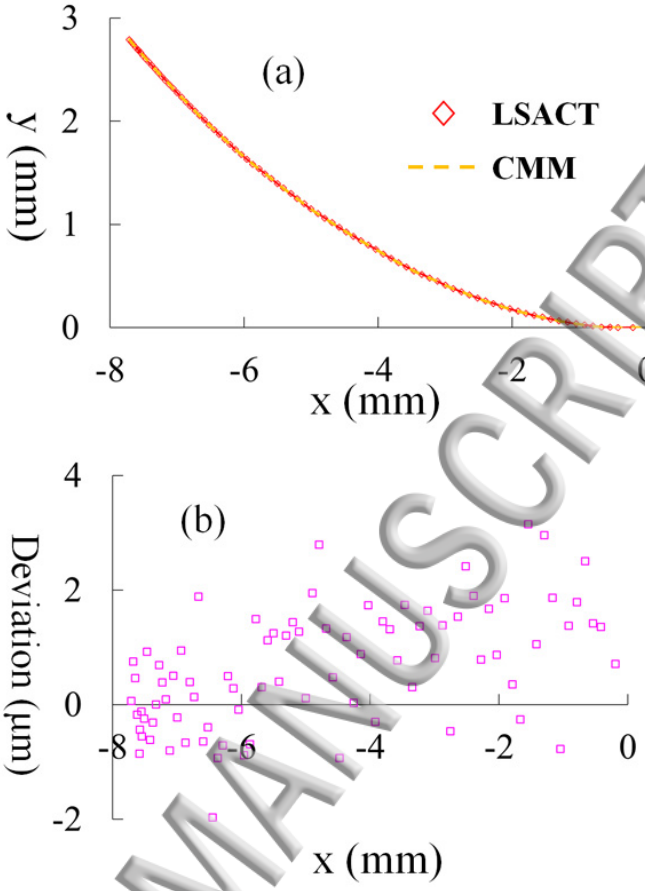

FIG. 7. Compared measured results of sample S_2 between LSACT and CMM. (a) Measured meridian line of sample S_2. The red hollow diamond represents the measured data from LSACT while the orange dotted line represents the measured curve from CMM. Coefficient of determination $C = 0.99999$ and $RMS = 1.213\ \mu m$. (b) The deviation of measured data from LSACT to the CMM. Using the standard aspheric equation (shown in caption of Fig. 4), the fitting coefficients $R = -11.184673, k = -0.249573, a = 4.019932 \times 10^{-5}, b = -8.784430 \times 10^{-8}, c = 2.731465 \times 10^{-9}$ for measured meridian line in CMM are obtained.

1-2 μm deviation from our LSACT and other reliable tester. In order to reduce the cost of designed instrument, the height of H, fixed value in whole measurement procedure, was measured by manual Caliper rather than a high-precision rail, which caused the obvious systematic error. The high-precision rail will be used in y-direction to measure the value of H for reduction of systematic error and improvement accuracy of the instrument in future work. On the other respect, the performance of the LSACT is also affected by several factors such as divergence of scanning beam reflected by the surface and and stray light incoming into PSD.

V. CONCLUSION AND DISCUSSION

In conclusion, this article presents a novel and simple technique for the testing of aspheric surfaces using geometrical optics metrology and analyzes appropriate algorithm used in tester for accurately restoring contour of the surfaces. The above experimental results, with coefficient of determination and RMS achieving 0.99999 and 1.5 μm, respectively, prove the capability of proposed LSACT to depict and reconstruct the surface with aspheric

shape in rapid rate. Moreover, although steep aspheric lens becomes hard to measure, our approach with long-range scanning makes it possible to measure samples with nearly 90^o slope in theory (see Eq. (1) and Eq. (2)). The reported LSACT, with 350 mm-long GGR and 75 mm maximum height of RM, will allow characterization of 150 mm-diameter steep surface with 75^o slope in border.

What is more, as a significant factor to access the performance of aspheric surface tester, measuring time is very often compromised at the precision. In LSACT, total measuring time is closed tied with the diameter of sample and sampling interval. With regard to single sampling point, measuring time mainly depends on the speed of step motor and rotatory motor, response time of PSD and data processing, which is fixed about 0.5 s. Optimizing the elements that consists of LSACT can potentially enables 0.3 s measuring time for single sampling point.

Distinct advantages for this instrument include simple and stable structure as well as high precision. Its highly flexible and low cost nature makes it a promising metrology technique for fabrication and manufacture of aspheric components, no matter steep or flat. When the sample is put on a rotary table, the new-design instrument can further be applied to shape specification for other special optical surfaces such as free-form surface, which facilitates the metrology of optical components. It is worth mentioning that non-diffracting beam[20] can be an alternative solution to combat severely diverging of light in scanning, which will further improve the accuracy of LSACT in future work.

[1] A. Yabe, Opt. Express **13**, 7233 (2005).
[2] R. A. Buchroeder, *Application of Aspherics for Weight Reduction in Selected Catadioptric Lenses* (Optical Sciences Center, University of Arizona, 1971).
[3] Y. H. Lo and R. Leonhardt, Opt. Express **16**, 15991 (2008).
[4] N. V. Chernomyrdin, M. E. Frolov, and S. P. Lebedev, Rev. Sci. Inst. **88**, 014703 (2017).
[5] S. Y. Li and Y. F. Dai, *Large and Middle-scale Aperture Aspheric Surfaces: Lapping, Polishing and Measurement* (Wiley-Blackwell, 2017).
[6] A. Beutler, Adv. Opt. Techn. **5**, 211 (2016).
[7] G. S. Khan, *Characterization of Surface Roughness and Shape Deviations of Aspheric Surfaces* (Friedrich-Alexander-Universitat Erlangen-Nurnberg, 2008).
[8] C. Tian, Y. Y. Yang, T. Wei, and Y. M. Zhuo, Appl. Optics **50**, 3559 (2011).
[9] J. C. Wyant and V. P. Bennett, Appl. Optics **11**, 2833 (1972).
[10] H. S. Yang, J. B. Song, I. W. Lee, and Y. W. Lee, Opt. Express **14**, 3247 (2006).
[11] P. Murphy, G. Forbes, J. Fleig, P. Dumas, and M. Tricard, Opt. Photonics News **14**, 38 (2003).
[12] C. W. Liang, H. S. Chang, P. C. Lin, C. C. Lee, and Y. C. Chen, Opt. Express **21**, 18255 (2003).
[13] P. Zhang, H. Zhao, X. Zhou, and J. Li, Opt. Express **18**, 15216 (2010).
[14] S. Chen, S. Li, Y. Dai, and S. Zeng, Opt. Express **16**, 4760 (2008).
[15] G. Ehret, M. Schulz, M. Stavridis, and C. Elster, Meas. Sci. Technol. **23**, 094007 (2012).
[16] K. Ishikawa, T. Takamura, M. Xiao, S. Takahashi, and K. Takamasu, Meas. Sci. Technol. **25**, 064008 (2014).
[17] M. Xiao, T. Takamura, S. Takahashi, and K. Takamasu, Precis. Eng. **37**, 599 (2013).
[18] M. Born and E. Wolf, *Principles of Optics* (Cambridge University Press, 1999).
[19] A. E. Ennos and M. S. Virdee, *Precision measurement of surface form by laser profilometr* (Wear, 1986).
[20] J. Durnin, J. Opt. Soc. Am. A **4**, 651 (1987).
[21] P. E. Murphy, T. G. Brown, and D. T. Moore, Appl. Optics **39**, 2122 (2000).
[22] G. Baer, J. Schindler, C. Pruss, J. Siepmann, and W. Osten, Opt. Express **22**, 31200 (2014).

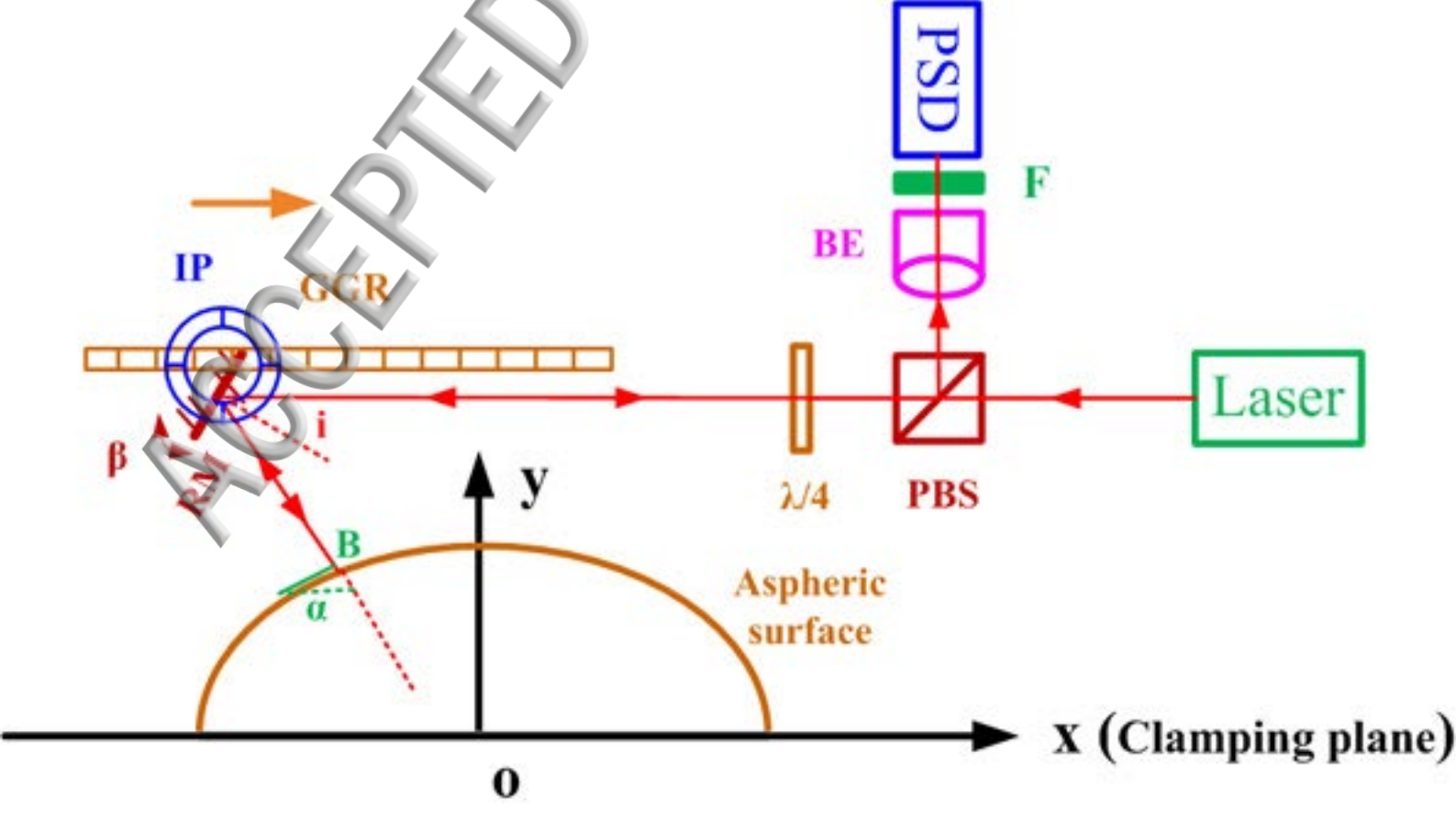
PSD
F
BE
IP
GGR
Laser
β
i
y
λ/4
PBS
B
α
Aspheric
surface
x (Clamping plane)
o

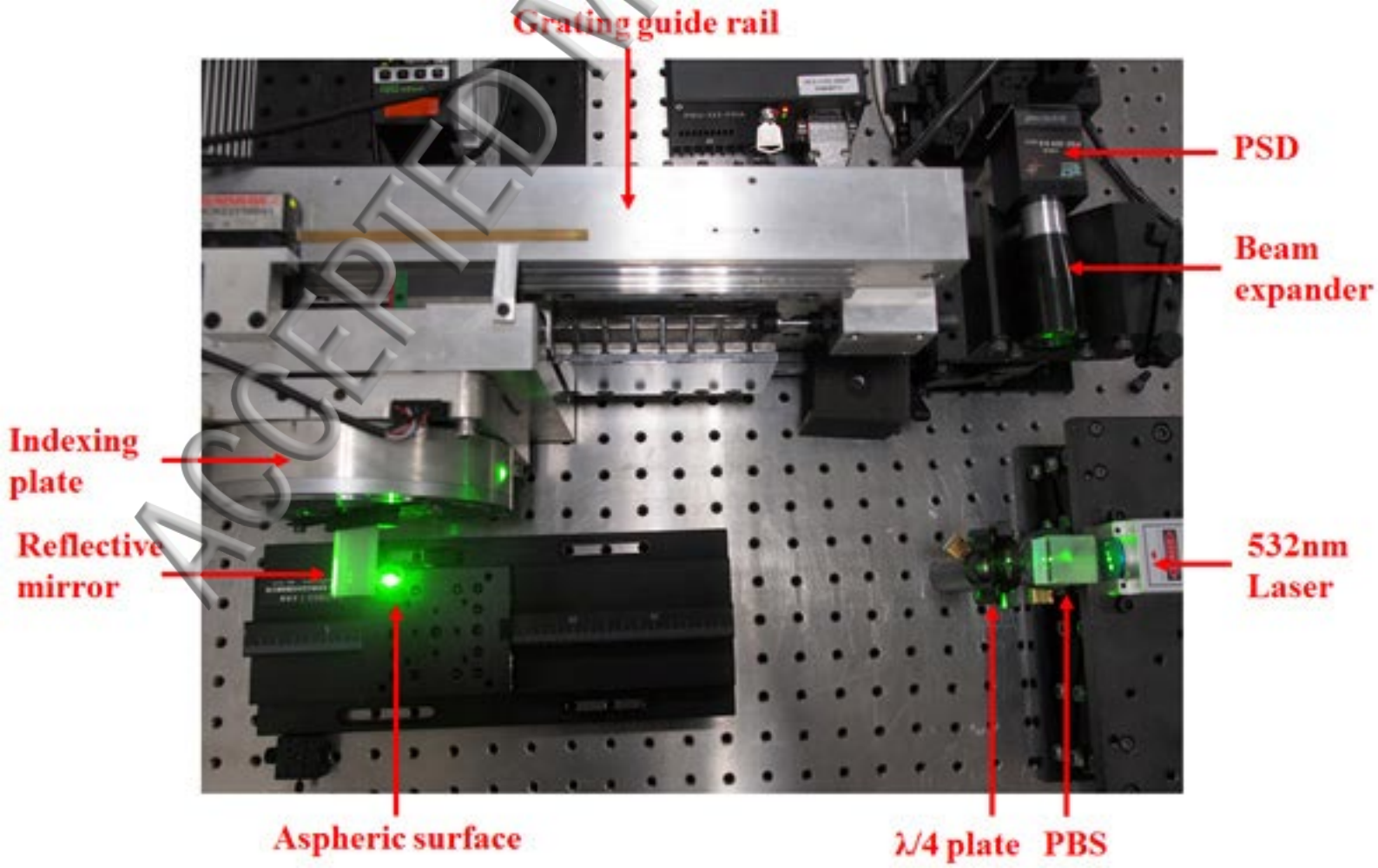
Grating guide rail
PSD
Beam expander
Indexing plate
Reflective mirror
532nm Laser
Aspheric surface
λ/4 plate
PBS

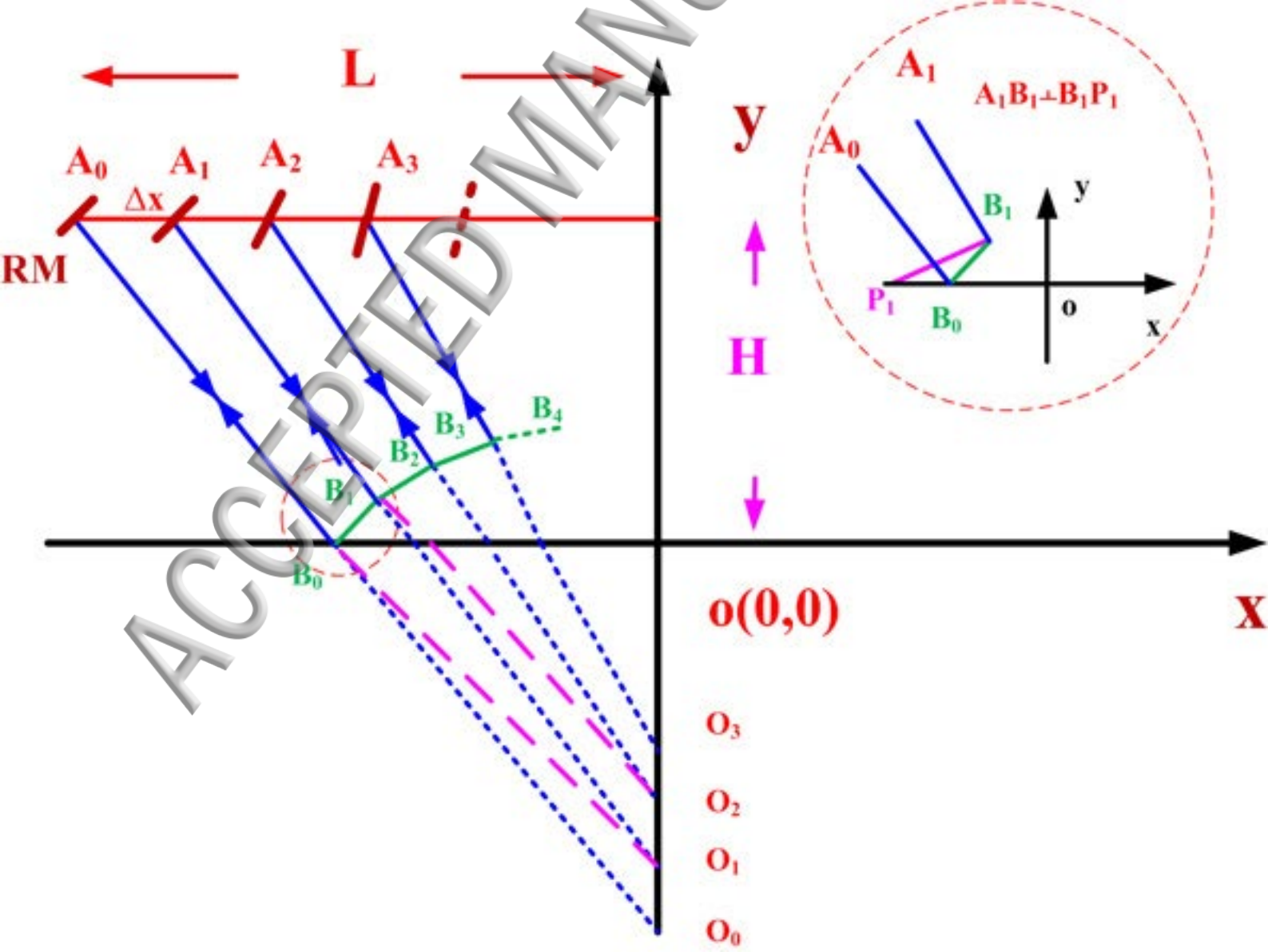

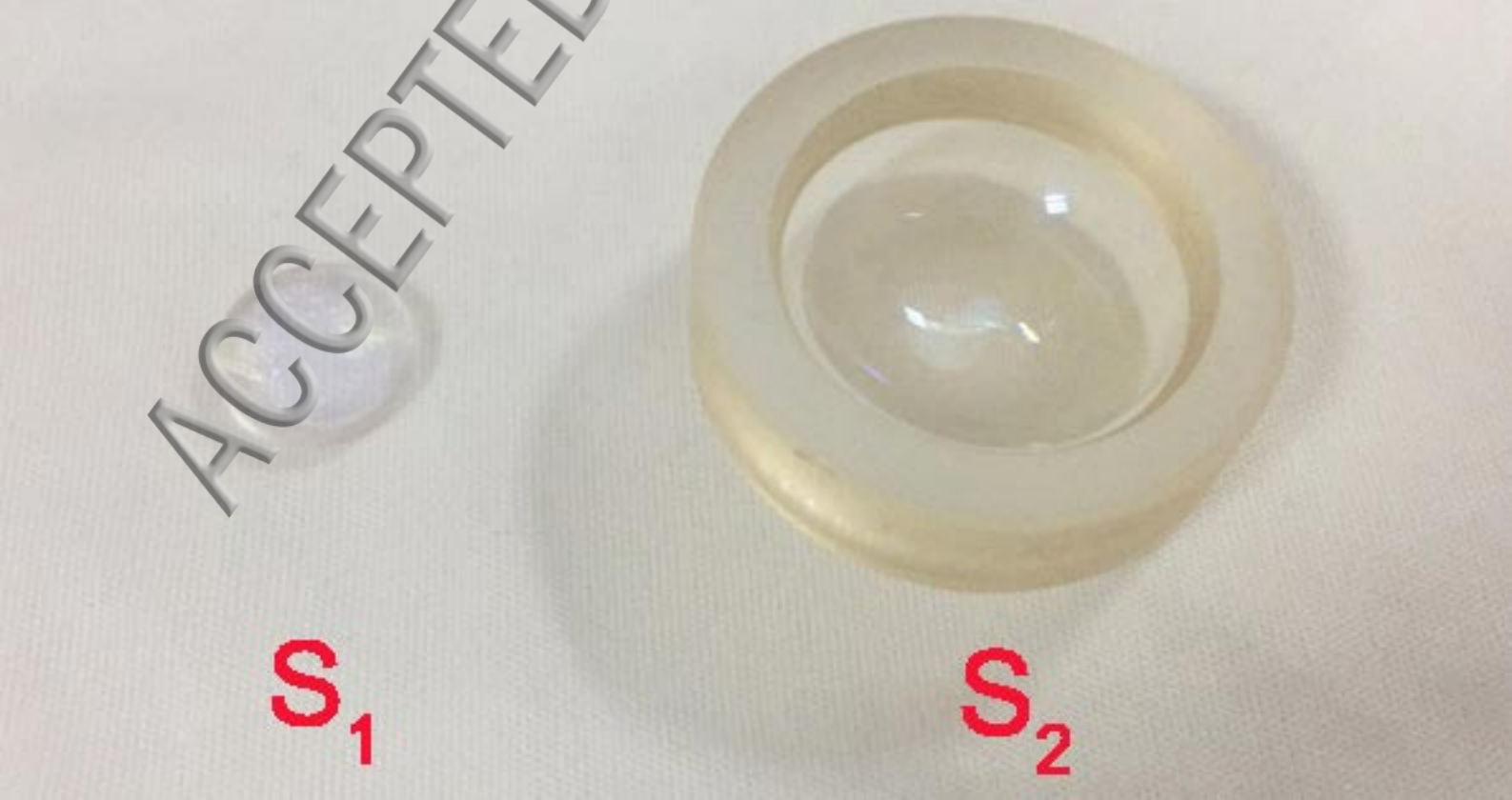
ACCEPTED
S1
S2